

Discovery of carbon-based strongest and hardest amorphous material

Shuangshuang Zhang^{1†}, Zihé Li^{1†}, Kun Luo^{1,2†}, Julong He^{1†}, Yufei Gao^{1,2†}, Alexander V. Soldatov^{3,4,5}, Vicente Benavides³, Kaiyuan Shi⁶, Anmin Nie¹, Bin Zhang¹, Wentao Hu¹, Mengdong Ma¹, Yong Liu², Bin Wen¹, Guoying Gao¹, Bing Liu¹, Yang Zhang^{1,2}, Dongli Yu¹, Xiang-Feng Zhou¹, Zhisheng Zhao^{1*}, Bo Xu¹, Lei Su⁶, Guoqiang Yang⁶, Olga P. Chernogorova⁷, Yongjun Tian^{1*}

¹Center for High Pressure Science (CHiPS), State Key Laboratory of Metastable Materials Science and Technology, Yanshan University, Qinhuangdao, Hebei 066004, China

²Hebei Key Laboratory of Microstructural Material Physics, School of Science, Yanshan University, Qinhuangdao 066004, China

³Department of Engineering Sciences and Mathematics, Luleå University of Technology, SE-97187 Luleå, Sweden

⁴Department of Physics, Harvard University, Cambridge, MA 02138, USA

⁵Center for High Pressure Science and Technology Advanced Research, Shanghai 201203, China

⁶Key Laboratory of Photochemistry, Institute of Chemistry, University of Chinese Academy of Sciences, Chinese Academy of Sciences, Beijing, 100190, China

⁷Baikov Institute of Metallurgy and Materials Science, Moscow 119334, Russia

* Corresponding authors: zzhao@ysu.edu.cn (Z.Z.) or fhcl@ysu.edu.cn (Y.T.). †These authors contributed equally to this work.

ABSTRACT

Carbon is likely the most fascinating element of the periodic table because of the diversity of its allotropes stemming from its variable (sp , sp^2 , and sp^3) bonding motifs. Exploration of new forms of carbon has been an eternal theme of contemporary scientific research. Here we report on novel amorphous carbon phases containing high fraction of sp^3 bonded atoms recovered after compressing fullerene C_{60} to previously unexplored high pressure and temperature. The synthesized carbons are the hardest and strongest amorphous materials known to date, capable of scratching diamond crystal and approaching its strength which is evidenced by complimentary mechanical tests. Photoluminescence and absorption spectra of the materials demonstrate they are semiconductors with tunable bandgaps in the range of 1.5-2.2 eV, comparable to that of amorphous silicon. A remarkable combination of the outstanding mechanical and electronic properties makes this class of amorphous carbons an excellent candidate for photovoltaic applications demanding ultrahigh strength and wear resistance. (153 words)

Keywords: amorphous carbon, ultrahard, ultrastrong, semiconductor, phase transition

INTRODUCTION

Contrary to the crystalline state of solid matter which is characterized by periodicity in the spatial organization of the constituting atoms, the amorphous state exhibits no long-range order in the atomic arrangement although certain well-defined structural motifs may be present over a few interatomic distances giving rising to a degree of short- to medium-range order[1]. The length scale over which such localized ordering occurs determines the physical properties for such systems. Another example is orientational disorder of molecules perfectly positionally arranged in a crystal. In both cases a common definition of the structure of these systems is disorder (spatial and/or orientational), which is also termed “glassy” state. Importantly, disordered systems exhibit many properties superior to their crystalline counterparts which makes them better candidates for technological applications. Bulk metallic glasses (BMG) have physical properties combining the advantage of common metals and glasses - strength several times higher than corresponding crystalline metals, good ductility and corrosion resistance[2]; hydrogenated amorphous silicon (a-Si:H) films exhibiting an optical absorption edge at ~ 1.7 eV have been the most popular photovoltaic semiconductor used in solar cells[3], and the a-Si:H/c-Si heterojunction-based solar cell has increased efficiency steadily to a current record value of 24.7%[4], to name just a few examples. Importantly, theoretical modeling of amorphous state is prohibitively difficult, thus exploring new amorphous states of matter and their nature is both rewarding and, at the same time, a very challenging scientific task of contemporary materials science.

Amorphous carbon exhibits a rich variety of physical properties determined by the (sp - sp^2 - sp^3) bonding character and structural motif of the constituting atoms. Graphite-like sp^2 carbon, for example, is conductive, highly compressible and flexible due to disordered stacking of graphene layers in clusters. On the contrary, sp^3 bonding-dominated diamond-like carbon (DLC) films prepared by different deposition techniques from a large variety of carbon-carrying precursors exhibit high hardness, chemical inertness, and tunable optical band gaps and, therefore, are

widely used as protective coatings[5–7]. However, very large intrinsic stresses of up to several GPa in DLC films may result in the delamination of thick films from the substrates, and thereby limit the application of DLC coatings[8, 9].

Amorphous carbon can be alternatively synthesized by compression of sp^2 carbon precursors, typically fullerenes and glassy carbon[10–18]. Although C_{60} molecules sustain pressure up to 20-25 GPa at ambient temperature[19], the buckyballs get easily broken already at about 5 GPa and elevated temperatures (≤ 800 °C) to form a disordered nano-clustered graphene-based hard phase with more than 90% elastic recovery after deformation[20, 21]. Likewise, disordered carbon materials with different sp^2 - sp^3 carbons ratios exhibiting a remarkable combination of lightweight, high strength and elasticity together with high hardness and electro-conductivity can be recovered after compressing glassy carbon at pressures of 10-25 GPa and high temperatures ≤ 1200 °C[10]. With further increase of pressure the glassy carbon transforms into a metastable sp^3 -rich dense, ultra-incompressible amorphous carbon[11–13]. Importantly, synthesis of carbon allotrope capable of scratching diamond by exposure of fullerene C_{60} to 13 GPa, 1227-1477 °C with subsequent quenching to ambient conditions has been reported[16], although properties of this phase and interpretation of its structure remain a subject of unresolved controversy. Even though the great efforts have already been put into exploration of the p , T phase diagram of C_{60} , the pressure range above 20 GPa, has yet to be established. As synthesis pressure strongly affects the microstructure and bonding in carbon phases produced from C_{60} , we may envisage emergence of new amorphous carbon polymorphs as a result of crystal-to-amorphous and/or amorphous-to-amorphous phase transitions[22, 23] triggered in the pressure range of the structural integrity of C_{60} .

Here, we present a systematic study of the behavior of C_{60} fullerene at previously unexplored pressure of 25 GPa and different temperatures. A new class of amorphous carbons were synthesized and characterized by complimentary techniques: X-ray diffraction (XRD), Raman spectroscopy, high-resolution

transmission electron microscopy (HRTEM), and electron energy loss spectroscopy (EELS). Our results demonstrate that the sp^3 carbon fraction in these materials gradually increases with increase of the synthesis temperature and, finally, reaches 43%-72%. Different hardness measurement methods including Knoop (H_K), Vickers (H_V) and nanoindentation hardness (H_N) together with uniaxial compressive strength test were employed in order to assure consistency of the obtained results and demonstrate that the synthesized *bulk* carbon-based material is the hardest and strongest amorphous material. In addition, unlike insulator diamond, these amorphous carbons are semiconducting with relatively narrow bandgap (1.5~2.2 eV) that opens up good perspectives for using this material in new class of photoelectric applications.

RESULTS AND DISCUSSION

Structural characterization

Fig. 1a shows XRD patterns of the materials recovered after treatment of C_{60} at 25 GPa and various synthesis temperatures. The following sequence of phase transitions was observed: first, C_{60} transforms into the known 3D polymer[16] at elevated temperature (new sharp diffraction peaks appear), then buckyballs destruction/structure amorphization begins at about 500 °C (very broad new peaks appear and the intensity of the polymer peaks decreases) and completes above 800 °C. The materials recovered from 1000 °C, 1100 °C and 1200 °C, termed as AM-I, AM-II and AM-III, respectively, are characterized by a dominant broad diffraction peak centered near $q \sim 3.0 \text{ \AA}^{-1}$, fairly close to the position of (111) reflection of diamond ($q = 3.05 \text{ \AA}^{-1}$) and a weaker peak at $q \sim 5.3 \text{ \AA}^{-1}$ (Fig. 1a and Fig. S1, Supplementary information (SI)), which represent an entirely new class of amorphous carbon distinctly different from the previously reported low-density amorphous phases synthesized at lower pressures and temperatures (13 GPa, 1227-1477 °C)[16]. Notably, the previously discovered amorphous carbons have another graphite-like diffraction peak near $q \sim 2.0 \text{ \AA}^{-1}$ indicating the large interlayer

spacing and lower density[17] (see also the results of our test experiment conducted at similar conditions as described in ref. 16, Fig. S2, SI). With the synthesis temperature increase from 1000 °C to 1200 °C, the amorphous peaks become slightly narrower and shift from ~ 2.88 to 3.00 \AA^{-1} , indicating further density increase. Accordingly, the position of first nearest neighbor peak in derived pair distribution functions $G(r)$ shifts to higher r from AM-I to AM-III, corresponding to an average bond length increase from 1.47 \AA to 1.50 \AA (Fig. S1, SI). The bond lengths of the AM carbons lie between the bond length of sp^2 (1.42 \AA) and sp^3 (1.55 \AA) carbons in graphene and diamond, respectively, thus demonstrating presence of both hybridizations in the AM carbons under investigation. Also, the material's color changes from opaque black to transparent yellow (insets in Fig. 1b). As the synthesis temperature exceeds 1300 °C, the narrow diffraction peaks corresponding to (111), (220) and (311) reflections of diamond appear near 3.05 , 4.98 and 5.84 \AA^{-1} , respectively, indicating the formation of nano-diamond coexisting with the remaining amorphous phase.

The bonding difference in the amorphous carbons is reflected in their Raman spectra (Fig. 1b and Fig. S3a, SI). The AM-I and AM-II carbons exhibit a broad Raman peak around 1600 cm^{-1} with full width at half peak maximum (FWHM) of $\sim 200 \text{ cm}^{-1}$, corresponding to G band characteristic of sp^2 carbons. Appearance of the G-band peak testifies for relatively high fraction of sp^2 bonded carbons[24]. Indeed, accounting for very low Raman cross-section for sp^2 carbons at UV laser excitation, the high intensity of the G-band in the spectra of AM-I and AM-II carbons clearly indicates on the sp^2 carbon dominance in these amorphous phases. Importantly, both position and the FWHM of the G-band peak indicate the Raman scatterers' (clusters) size in these phases must be less than 2 nm [25]. On the contrary, the background-subtracted Raman spectrum of the AM-III carbon reveals several new features. First, a band located at the low wavenumbers of $900\sim 1300 \text{ cm}^{-1}$ (termed as "T band"[25]) is a characteristic signature of sp^3 carbons and thus indicates on their high concentration in the AM-III phase. Second, an evident shoulder (rising peak) on

high frequency side of the G-band (at 1740 cm^{-1}) may be attributed to clustering (cross-linking via sp^3 bonds) of remaining aromatic rings formed of sp^2 carbons and, finally, the peak appearing at about 1930 cm^{-1} is likely originating from short linear chains (Fig. S3b, SI). After completion of the AM–diamond transformation above $1600\text{ }^{\circ}\text{C}$, the fingerprint peak of crystalline diamond at $\sim 1330\text{ cm}^{-1}$ appears in the spectra of transparent diamond samples (see inset in Fig. 1b).

In order to confirm the microstructure and bonding nature of the amorphous phases suggested by Raman, HRTEM, selected area electron diffraction (SAED) and EELS were performed. The SAED patterns display two diffuse rings near $2.1\text{ }\text{\AA}$ and $1.2\text{ }\text{\AA}$ in all three amorphous carbon materials (Fig. 2), that is consistent with the XRD results. For comparison, the composite sample recovered from $1300\text{ }^{\circ}\text{C}$ shows, in addition, the “spotty” diffraction rings indicating the formation of nanocrystalline diamond. Carbon K-edge EELS are shown in Fig. 2e-g and Fig. S4, and S5b (SI). The main feature of the low EELS data is a gradual shift of the plasmon peak from its position in pristine C_{60} (26.0 eV) to higher energies in AM-I, AM-II and AM-III (29.7 , 30.7 , and 32.8 eV , respectively) that demonstrates increase of sp^3 fraction in the amorphous phases. Using C_{60} as a reference, pure sp^2 material, we estimated sp^3 fraction in AM-I, AM-II, AM-III and AM/diamond composite at $43\pm 3\%$, $50\pm 2\%$, $72\pm 2\%$ and $85\pm 2\%$, respectively. The plasmon peak position in AM-III phase is higher than that in the “amorphous diamond” produced by quenching glassy carbon from high p, T[11] (31.8 eV) that implies lower sp^3 content and density in the latter. In addition, the area of EELS peak at 285 eV signaling the sp^2 bonds fraction in the material gradually decreases when going from AM-I to AM-III phase (Fig. S4, SI). The linear EELS scans with high spatial resolution in randomly selected sample regions demonstrate the bonding homogeneity at least on 1 nm scale in these AM phases (Fig. 2f, g). The subtle microstructure differences between the AM phases are further revealed by HRTEM images that exhibit a characteristic “worm-like” contrast manifesting structural disorder (Fig. 2a-c). The dimensions of these very fine structural fragments gradually decrease with the synthesis temperature increase,

reaching statistically averaged size of about 12 Å, 8 Å and only 4 Å in AM-I, AM-II and AM-III, respectively. That clearly distinguishes these disordered carbon phases from those containing substantially lower fraction of sp^3 -bonded atoms obtained from glassy carbon at similar p, T conditions[10], underscoring importance of the precursor material selection in high p, T synthesis. Such small structural fragments, presumably highly interlinked via sp^3 carbons makes AM-III with directly measured density of $\sim 3.35 \pm 0.1$ g/cm³ (comparable to that of diamond) the densest amorphous carbon.

Mechanical properties

The hardness values, i.e. H_K , H_V and H_N , of the amorphous carbon materials were estimated by three independent measurement methods. The results as well as detailed indentation images are present in Fig. 3 and Figs. S6 and S7 (SI). Among the synthesized materials, AM-III has the highest hardness of $H_K = 72 \pm 1.7$ GPa and $H_V = 113 \pm 3.3$ GPa, whereas the AM-I and AM-II have H_K of 58 ± 1.9 and 62 ± 1.9 GPa, respectively. In comparison, the H_V and H_K values of (111) plane of natural single crystalline diamond are 62 and 56 GPa[26, 27], respectively (Fig. 3a and Fig. S8, SI) thus hardness of the synthesized amorphous carbons can rival that of diamond. Careful analysis of Vickers indentation morphologies of AM-III shows that the raised “pile-up” was formed due to flow of the displaced material up around the indenter, indicating the plastic character of the deformation during loading (Fig. S9c, SI). With the applied load increase up to 3.92 N, the radial and lateral cracks as well as the peeling zone can be observed around the resultant indentations (Fig. S9a, b, SI), implying occurrence of the plastic-to-brittle transition in the material[28]. Moreover, the H_N and Young’s modulus (E) have also been determined based on the load-displacement curves using Oliver and Pharr model[29] (Fig. S7, SI). The estimated E of AM-I, AM-II and AM-III are 747 ± 66 , 912 ± 89 , 1113 ± 110 GPa, respectively. The obtained H_N for them are 76 ± 3.4 , 90 ± 7.9 , and 103 ± 2.3 GPa, respectively, which are comparable to their Vickers hardness. Notably, the indentation hardness of AM-III exceeds the H_N record of 80.2 GPa held until now by

tetrahedral amorphous carbon (ta-C) films[7]. Such extreme hardness allows the AM-III sample scratch the (001) face of synthetic diamond crystal with Vickers hardness of 103 GPa (Fig. 3c and Fig. S8a, SI). Possessing hardness comparable to that of single crystalline diamond this class of amorphous carbon becomes the hardest amorphous material known to date (Fig. 3b). More significantly, the advantage of this type of ultrahard amorphous carbon is that they have isotropic hardness comparable to diamond crystals where the hardness varies along different crystallographic directions leading to a cleavage of diamond easy to occur along its “weak” crystal planes.

The superior mechanical properties of the amorphous carbon materials have been further demonstrated by *in-situ* uniaxial compression/decompression test (Fig. S10, SI). It was found that micron-sized pillar made out of the AM-III phase with top diameter of 0.88 μm has compressive strength of at least 40 GPa, and could be fully elastically recovered without fracture after decompression at ambient conditions. Subsequent measurement of a micron-sized pillar with larger top diameter (3.78 μm) demonstrated its ability to withstand compressive stress as high as ~ 70 GPa without fracture (Fig. 4a) although in this case a closer examination of the decompressed pillar revealed some wrinkles produced in its upper part, very similar to the shear bands formed in metallic glasses during deformation[30]. Another AM-III micron-sized pillar with diameter of 2.64 μm was broken at stress load of 65 GPa before reaching its strength limit. Thus the measured compressive strength of AM-III material lies in between that of $\langle 100 \rangle$ - and $\langle 111 \rangle$ -oriented diamond micron-pillars exhibiting the compressive strength of ~ 50 GPa and ~ 120 GPa, respectively[31]. Theoretically, the maximum compressive strength of materials can only be obtained when the compression direction is strictly parallel to the normal to the measured sample surface, the condition which is very difficult to achieve. As a result, the value of ideal compressive strength of the amorphous carbon pillars should, in fact, be higher than that we determined in our experiment. Consequently, our measurements demonstrate that the AM-III material is comparable in strength to

diamond and superior to the other known strongest materials (Fig. 4b).

It is important to ascertain what may be the reason(s) for the observed AM carbon phases with sp^3 carbon fraction still far below 100%, in particular AM-I with only 43% sp^3 , exhibiting hardness and strength comparable to that of crystalline diamond. Indeed, it is well known, the sp , sp^2 and sp^3 covalent bonds in elemental carbon are all extremely strong. For example, the intrinsic strength of graphene (pure sp^2 carbon) reaches a value as high as 130 GPa[32] thus exceeding ultimate shear strength of diamond (95 GPa[33]) comprised of sp^3 carbons. The fundamental reason for the softness of graphite is weak van der Waals interaction between graphene layers. However, high pressure induces partial sp^2 -to- sp^3 transformation leading to interlinking/locking-in the graphene layers by the tetrahedral sp^3 bonds and profound increase of hardness and strength of the resulting high-pressure phase that is able to abrade the diamond anvils[34]. Such sp^2 - sp^3 carbon system with only 22% sp^3 fraction experimentally obtained at ambient conditions by quenching from high-pressure compressed glassy carbon has high hardness of 26 GPa[10], whereas the three-dimensional (3D) C_{60} polymer comprised of covalently linked (via sp^3 bonds) fullerene molecules with 40% sp^3 carbons content, possesses superhigh hardness of 45 GPa[35]. Moreover, a number of superhard/ultrahard sp^2 - sp^3 crystalline carbon forms were recently predicted theoretically. For example, the carbons designated as P-1-16b, P-1-16e, and P-1-16c with ~50% sp^3 carbons are predicted to have ultrahigh hardness of 71.3-72.4 GPa[36], and a series of superhard sp^2 - sp^3 3D carbon nanotube polymers such as the 3D (8,0) nanotube polymer with 43.5% sp^3 carbons is predicted to have superhigh hardness of 54.5 GPa[37, 38]. All the above mentioned experimental and theoretical results demonstrate that ultrahigh hardness and strength comparable to crystalline diamond can be achieved in sp^2 - sp^3 carbon systems at sp^3 concentrations far below 100%. The AM carbons synthesized in this work have higher sp^3 contents than that in compressed glassy carbon[10] and 3D- C_{60} polymers[35] thus we may anticipate higher hardness and strength in our systems. More importantly, it's not just a fraction of sp^3 carbon atoms that matters in this case

but the structural motif. We argue that our sp^2 - sp^3 carbon systems represent a particular short-range order which is a “blend” of remaining sp^2 carbon-based units (fused aromatic rings, short chains) covalently interlinked with clusters of tetragonally-coordinated sp^3 carbons. Such a “blend” represented on the HRTEM images (Fig. 2 a-c) by a worm-like structural fragments must combine nearly intrinsic graphene-type strength/hardness of the sp^2 units with diamond-like strength/hardness of the clusters formed by tetragonally-coordinated sp^3 carbons. That may explain why already AM-I carbon with relatively low sp^3 fraction is competitive in hardness and strength with crystalline diamond. On developing of substantially smaller structural fragments (fused rings opening, interlinking the structural units via short chains) along with significant increase of sp^3 fraction in AM-III carbon, a new short-range order must emerge and further manifest in profound increase of hardness, strength and altering the optical properties of the system.

Optical properties

These amorphous carbon materials under investigation display also unusual optical properties. Through at a wavelength of 532 or 633 nm laser excitation, all the materials exhibit strong photoluminescence (PL) in range of 550-950 nm (Fig. 5a). The PL maxima correspond to photon energy of 1.59 ± 0.1 , 1.74 ± 0.2 and 1.87 ± 0.1 eV, in AM-I, AM-II, AM-III phases, respectively. This difference is directly related to the higher content of sp^3 carbon-based material possessing larger bandgaps in the samples. In view of yellow-transparent nature of AM-III, its visible light absorption spectrum was measured in transmission utilizing a diamond anvil cell (DAC). The inset of Fig. 5b shows the view in transmitted light through a sample piece mounted in a gasket hole inside the DAC. The result indicates that the optical absorption edge of AM-III is located at the ~ 570 nm, which corresponds to a bandgap of 2.15 eV, consistent with the PL results. Therefore, the amorphous carbons are a class of semiconductors with bandgaps less than diamond (5.5 eV) and close to amorphous silicon (a-Si:H) films (~ 1.7 eV) widely used in technology nowadays. The preferable

optical bandgaps offer a potential of using these amorphous carbons as optimal semiconductors for novel photoelectric applications.

Comparison of various types of amorphous carbon

It is important to define position of the materials we produced on the current landscape of other technologically important (hard) amorphous carbon-based materials. All the data reported/published to date can be divided into 2 categories: thin films prepared by various deposition routes[7, 25, 39, 40] and the materials synthesized at high-pressure and high-temperature using different precursors such as fullerene[16, 41] and glassy carbon (GC)[10–13]. *Further we mainly focus on the most distinct material – AM-III* (Fig. 6). Comparing, for example, the microstructure and bonding of the discovered AM-III to ta-C/ta-C(:H) films[7, 25, 39, 40] through the correspondent UV Raman and EELS (Fig. 6a, b), one can see a much stronger Raman T band around $900\sim 1300\text{ cm}^{-1}$ characteristic of sp^3 carbons and a negligible EELS intensity in the AM-III against the peak near 285 eV representing residual sp^2 carbons in ta-C/ta-C(:H) films[39, 40]. Importantly, the residual sp^2 carbons present in the films in the form of orientationally disordered nano-sized graphene clusters whereas no graphene-based structural units survive 25 GPa synthesis pressure in AM-III we report here. The evident structural difference results in significant performance difference between these materials. For example, the AM-III has a high indentation hardness of 103 GPa, which is comparable to the hardest crystal plane of diamond, and higher than that (80.2 GPa) of the reported “hardest” ta-C film[7].

In the second category, the hard amorphous carbon materials were produced at high p, T from fullerene and glassy carbon (GC) precursors with synthesis pressures up to 15 GPa[16, 41] and 50 GPa[11], respectively. The XRD patterns in Fig. 6c exhibit clear difference between AM-III and various AM carbon phases synthesized previously by compressing C_{60} at relatively low synthesis pressures (up to 15 GPa)[16, 41] - the graphite-like diffraction peaks near $q=1.5\text{-}2.0\text{ \AA}^{-1}$ still appear in the XRD patterns indicating presence of large interlayer spacings and, consequently, relatively

low densities. These highly-disordered sp^2 carbon-based systems exhibit graphene nanoclusters-derived short range-order that is preserved at the synthesis pressure used in earlier experiments which is evidenced in both Raman and HRTEM data^{16,40}. In order to further reveal the difference between the AM carbons reported in this study and produced earlier we undertook a special effort and performed synthesis at p, T conditions (15 GPa, 550-1200 °C, see Fig. S2) similar to those used in Ref. 16. Apparently the Vickers hardness of the material we synthesized at 15 GPa, 800 °C (see its HRTEM in Fig. 6d) was found to be 68 GPa, i.e. lower than that of newly discovered AM carbons (Fig. 3a). Thus: i) testifying for presence of an entirely different type of short-range order and composition (sp^2/sp^3 ratio) in the latter systems and ii) demonstrating that fullerene compression at a level of 25 GPa is an essential requirement to facilitate both altering the short-range order (crushing the residual nano-graphene clusters) and sp^2 to sp^3 transformation/formation of the tetragonal amorphous carbon matrix. On the contrary, using GC comprised of relatively large, irregular and curved multilayer graphene sheets as the precursor demonstrated that one must go to much higher pressure than 25 GPa in order to create sp^3 carbon-based material as graphene nanoclusters formed by crushing the curved graphene sheets in GC survive at this synthesis pressure and exhibit super-elastic properties when quenched to ambient conditions[10]. Indeed, laser heating to ~1527 °C at 50 GPa allowed to produce a sp^3 -rich system, so called “quenchable amorphous diamond” (a-D)[11]. It is important to underscore the big difference between microstructures of the sp^3 carbon-based AM phases we synthesized from compressing C₆₀ and a-D[11] which is evident from HRTEM images - very high structural homogeneity with uniform and ultrafine structural units/fragments in the former (Fig. 2a-c and Fig. 6f) and non-uniform, inhomogeneous contrast with larger size structural fragments overlapping with an additional contrast from crystalline planes with low spacing planes in the latter (Fig. 6e). In addition, XRD pattern of a-D reveals the signature of a residual peak at about 2 Å⁻¹ corresponding to graphite-like interlayer distance and low EELS data indicate higher residual sp^2 carbon contents in a-D compared to that in AM-III (Fig. 6c and Fig.

S5). That underscores clear difference between these amorphous carbon forms. The comparison of amorphous phases produced from GC to the materials synthesized in this work demonstrate ultimate importance of the precursor material in the high p, T synthesis. Indeed, using highly symmetrical intrinsically nanostructured C₆₀ molecule (only ~7 Å in diameter) as a precursor provides uniform bonds breaking and conversion along with amorphization of the structure under 25 GPa, 1000-1200 °C compared to GC where even pressure increase to 50 GPa was insufficient to turn it at ~1527 °C into a uniform *sp*³ carbon-based structure.

The above analysis demonstrates that the discovered AM carbons are indeed new materials never detected and reported before. Their distinct short-range order, microstructure and composition provide a unique combination of semiconducting electronic structure with superior mechanical properties (with hardness and strength at the level of natural/synthetic diamond in the AM-III phase), and undoubtedly demonstrate a new class of amorphous carbon material we produced.

Going further we must underscore that contrary to crystalline materials where using just one technique, XRD, for example is sufficient for distinguishing different structural states a complimentary characterization of the amorphous material is mandatory as it allows for clear identification of different states of disordered matter. Only using complimentary characterization comprised of XRD, Raman, HRTEM and EELS allowed us not only to distinguish the newly synthesized AM carbon phases from all other AM carbon materials reported to date but also to reveal subtle differences between these novel structural forms of carbon. For example, whereas the difference between AM-III and AM-I/AM-II phases is evident the latter phases are hard to distinguish when we look just at their Raman spectra (Fig. 1b and Fig. S3, SI). On the contrary, the EELS data indicate the difference in *sp*³ fraction between all the AM carbons (Fig. 2e-g and Fig. S4, SI), and the HRTEM demonstrates the homogeneous contrast but distinct difference in the size of the structural worm-like fragments in the AM carbons (Fig. 2a-c). We infer that evolution from AM-I to AM-II state likely goes via relaxation of the structure around crushed buckyballs triggered

by temperature increase at 25 GPa - fusion of the remaining aromatic rings built of sp^2 carbons, further carbon conversion from sp^2 to sp^3 state and bridging the fused rings and clusters of tetragonally-coordinated sp^3 atoms. A more profound change in the short-range order occurs in AM-III phase leading to the aromatic rings opening, short chains formation (evidenced by appearance of new Raman peak at 1940 cm^{-1} , Fig. S3b) and accompanied by interlinking of the structural elements via sp^3 carbons which fraction substantially increases on this step. Consequently, these structural differences result in different performance of the AM carbons, in particular, mechanical and optical, properties as discussed in detail above.

CONCLUSION

In summary, by extending synthesis pressure to 25 GPa a new class of amorphous carbon materials was created from C_{60} precursor. Higher synthesis pressure seizes growth of graphene clusters after buckyballs collapse leading to high enrichment of the synthesized disordered phases with sp^3 -bonded carbons thus concluding the search for a bulk material based on tetragonally-arranged sp^3 carbon network finally complimenting and expanding technological value of the existing 2D systems – ta-C and DLC films. Consequently, the materials exhibit outstanding mechanical properties – comparable to crystalline diamond, their hardness and strength surpass any known amorphous materials. Thermal stability of AM-III carbon in-air is comparable to that of diamond crystals[26] (Fig. S11, SI). Remarkably, these amorphous carbons are all semiconductors with the band gaps in the range of 1.5-2.2 eV. The emergence of this type of ultrahard, ultrastrong, semiconducting amorphous material offers excellent candidates to most demanding practical applications and calls-up for further experimental and theoretical exploration of the amorphous carbon allotropes. (4456 words)

METHODS

Sample synthesis

The amorphous carbon materials were recovered after compressing C_{60} fullerene (99.99%, Alfa Aesar) at pressure of 25 GPa at high temperatures. Each synthesis temperature required a

separate experiment with a new C_{60} sample (but from the same source batch). The C_{60} powder was firstly compacted and placed into a h-BN capsule with 1.2 mm inner diameter and 2.0 mm length, and then assembled into a hole in the center of 8-mm-spinel ($MgAl_2O_3$) octahedron with a Re heater and a $LaCrO_3$ thermal insulator. This assembly was the standard COMPRES 8/3 used for high-pressure ($P \sim 25$ GPa) and high temperature ($T \sim 2300$ °C) experiments in a large-volume multi-anvil press at Yanshan University, similar to the method described elsewhere[26]. Pressure loading/unloading rates were 2 GPa/hour. When the target pressure was reached, the sample was heated with a rate of 20 °C /min to peak temperature, maintained for 2 hours and finally quenched by turning off the electric power supply. The recovered sample rods were ~ 1 mm in diameter and 1.2-1.7 mm in height. The densities were directly estimated based on the mass and volume of samples.

X-ray diffraction

The structure of recovered samples was investigated by X-ray diffraction (XRD) with Cu $K\alpha$ radiation source (diffractometer: Bruker D8 Discover). In addition, *In-situ* angle dispersive XRD measurements were performed at the 4W2 High-Pressure Station of Beijing Synchrotron Radiation Facility (BSRF) and BL15U1 Hard x-ray micro-focus beamline of Shanghai Synchrotron Radiation Facility (SSRF).

Raman spectroscopy

Both Raman scattering and photoluminescence (PL) measurements were carried out on a Horiba Jobin–Yvon LabRAM HR-Evolution Raman microscope at ambient conditions. The Raman spectra were excited by the laser radiation of 325 nm, and the PL spectra were excited by 532 or 633 nm laser. In all experiments the laser beams was focused to a spot size of ~ 1 μm . The fluorescence background in spectra was subtracted using the LabSpec5 software (HoribaJobin Yvon, 2004 and 2005).

HRTEM and EELS measurements

The samples for HRTEM were prepared by a Ga focused ion beam (FIB) (Scios, FEI) milling with an accelerating voltage of 30 kV. The pieces with size of $\sim 10 \times 8 \times 2$ μm were firstly pre-cut from the bulk samples by using current of 30 nA, then ion beam current from 7, 5, 3, 1, 0.5, to 0.1 nA was used in sequence to further mill the pieces to electron-transparent slices with thickness of less than 100 nm. After that the ion cleaning for about 10 minutes was applied to each side of slice under a voltage of 5 kV and current of 16 pA to minimize the knock-out damage on the slices. HRTEM, SAED, and EELS measurements were carried out at Themis Z TEM, using accelerating voltage of 300 kV. The EELS spectra were collected in the TEM mode at a random region of ~ 200 nm, and the sp^2/sp^3 fractions were estimated from the EELS data using the spectrum of pristine C_{60} as a reference, similar to the method described elsewhere[10]. The EELS line scans were conducted in STEM mode with an energy resolution of 0.6 eV and spatial resolution of ~ 1 nm.

Hardness and elastic modulus measurement

The Knoop hardness (H_K) and Vickers hardness (H_V) were measured by microhardness tester (KB 5

BVZ), and the adopted loading and dwelling time were 40 s and 20 s, respectively. For each sample, at least 5 indentations were performed at different loads from 0.98 to 3.92 N, in order to obtain the asymptotic hardness values. H_K was determined from $H_K=14229P/d_1^2$, where P (N) is the applied load and d_1 (μm) is the major diagonal length (long axis) of rhomboid-shaped Knoop indentation. H_V was determined from $H_V=1854.4P/d_2^2$, where d_2 (μm) is the arithmetic mean of the two diagonals of Vickers indentation. The scratch test was also conducted by using AM-III carbon as an indenter to scratch the (001) crystal face of diamond. Nanoindentation hardness (H_N) were measured at the peak load of 0.98 N with a three-sided pyramidal Berkovich diamond indenter (Keysight Nano Indenter G200), and the loading and dwelling times were both 15 s. The Young's moduli (E) were derived from the loading/unloading-displacement curves according to the Oliver-Pharr method[29]. The indentations were imaged by the Atomic Force Microscope (AFM) to obtain the accurate hardness.

Compressive strength test

The micron-pillars with diameters of ~ 1 to $4\ \mu\text{m}$ and aspect ratios of ~ 1.5 to 2.5 were fabricated using a Ga ion beam at an accelerating voltage of 30 kV in FIB instrument (Scios, FEI). The current of 30 nA was firstly used to mill a large crater, and in its center a micron-pillar with more than twice the targeted diameter was milled simultaneously. Then, the desired size of micron-pillar was achieved by polishing the coarse micron-pillar with low currents from 1000, 500, 300, 100, to 30 pA in turn, in order to minimize the irradiation damage. The compression measurements were conducted at two independent instruments, i.e. PI 87 PicoIndenter system interfaced with a Helios NanoLab DualBeam microscope, and nanoindentation system (Keysight Nano Indenter G200), respectively. The PI 87 PicoIndenter system was used to measure the small micron-pillars of $\sim 1\ \mu\text{m}$ by using a diamond flat punch ($5 \times 5\ \mu\text{m}$). The maximum load that the instrument can bear was 30 mN, and the used loading rate was 2 nm/s. For larger micron-pillars, the nanoindentation system was used because it can support large loads up to 9.8 N, and a $40 \times 40\ \mu\text{m}$ flat diamond punch was adopted during compression with a loading rate of 2 mN/s.

Optical absorption

The VIS/NIR absorption spectra were recorded on a UV/VIS/IR spectrometer (Avantes, AvaSpec) using a Xenon Light Source. A small piece of the AM-III sample with $\sim 50\ \mu\text{m}$ thickness was confined in a $400\text{-}\mu\text{m}$ -diameter hole pre-drilled in T301 gasket which was subsequently mounted in a diamond-anvil cell (DAC) for visible light absorption measurements. The band gaps were derived from the absorption spectra using the method described elsewhere[42].

Thermal stability measurement

Differential scanning calorimetry (DSC) and thermogravimetric analysis (TGA) using NETZSCH STA 449F5 were measured in the temperature range of 25-1400°C with heating rate of 10 °C/min. (1022 words)

REFERENCES

1. Machon D, Meersman F, and Wilding MC, *et al.* Pressure-induced amorphization and

- polyamorphism: Inorganic and biochemical systems. *Prog Mater Sci* 2014; **61**: 216–282.
2. Wang WH, Dong C, Shek CH. Bulk metallic glasses. *Mater Sci Eng R Rep* 2004; **44**: 45–89.
 3. Streer RA. Technology and applications of amorphous silicon. *Springer, Berlin* 2000.
 4. Taguchi M, Yano A, and Tohoda S, *et al.* 24.7% record efficiency HIT solar cell on thin silicon wafer. *IEEE J Photovolt* 2014; **4**: 96–99.
 5. Robertson J. Diamond-like amorphous carbon. *Mater Sci Eng R Rep* 2002; **37**: 129–281.
 6. Grill A. Diamond-like carbon: State of the art. *Diam Relat Mater* 1999; **8**: 428–434.
 7. Friedmann TA, Sullivan JP, and Knapp JA, *et al.* Thick stress-free amorphous-tetrahedral carbon films with hardness near that of diamond. *Appl Phys Lett* 1997; **71**: 3820–3822.
 8. Gioti M, Logothetidis S, Charitidis C. Stress relaxation and stability in thick amorphous carbon films deposited in layer structure. *Appl Phys Lett* 1998; **73**: 184–186.
 9. Angus JC, Hayman CC. Low-pressure, metastable growth of diamond and “diamondlike” phases. *Science* 1988; **241**: 913–921.
 10. Hu M, He J, and Zhao Z, *et al.* Compressed glassy carbon: An ultrastrong and elastic interpenetrating graphene network. *Sci Adv* 2017; **3**: e1603213.
 11. Zeng Z, Yang L, and Zeng Q, *et al.* Synthesis of quenchable amorphous diamond. *Nat Commun* 2017; **8**: 322.
 12. Lin Y, Zhang L, and Mao H, *et al.* Amorphous diamond: A high-pressure superhard carbon allotrope. *Phys Rev Lett* 2011; **107**: 175504.
 13. Yao M, Xiao J, and Fan X, *et al.* Transparent, superhard amorphous carbon phase from compressing glassy carbon. *Appl Phys Lett* 2014; **104**: 021916.
 14. Wang L, Liu B, and Li H, *et al.* Long-range ordered carbon clusters: A crystalline material with amorphous building blocks. *Science* 2012; **337**: 825–828.
 15. Soldatov AV, Roth G, and Dzyabchenko A, *et al.* Topochemical polymerization of C₇₀ controlled by monomer crystal packing. *Science* 2001; **293**: 680–683.
 16. Blank VD, BuGA SG, and Dubitsky GA, *et al.* High-pressure polymerized of C₆₀. *Carbon* 1998; **36**: 319–343.
 17. Álvarez-Murga M, Hodeau JL. Structural phase transitions of C₆₀ under high-pressure and high-temperature. *Carbon* 2015; **82**: 381–407.
 18. Shibazaki Y, Kono Y, Shen G. Compressed glassy carbon maintaining graphite-like structure with linkage formation between graphene layers. *Sci Rep* 2019; **9**: 7531.
 19. Duclos SJD, Brister K, and Haddon RC, *et al.* Effects of pressure and stress on C₆₀ fullerite to 20 GPa. *Nature* 1991; **351**: 380–382.
 20. Wood RA, Lewis MH, and West G, *et al.* Transmission electron microscopy, electron

diffraction and hardness studies of high-pressure and high-temperature treated C₆₀. *J Phys Condens Matter* 2000; **12**: 10411–10421.

21. Chernogorova O, Potapova I, and Drozdova E, *et al.* Structure and physical properties of nanoclustered graphene synthesized from C₆₀ fullerene under high pressure and high temperature. *Appl Phys Lett* 2014; **104**: 043110.
22. McMillan PF, Wilson M, Daisenberger D, Machon D. A density-driven phase transition between semiconducting and metallic polyamorphs of silicon. *Nat Mater* 2005; **4**: 680–684.
23. Daisenberger D, Wilson M, and McMillan PF, *et al.* High-pressure x-ray scattering and computer simulation studies of density-induced polyamorphism in silicon. *Phys Rev B* 2007; **75**: 224118.
24. Beeman D, Silverman J, Lynds R, Anderson MR. Modeling studies of amorphous carbon. *Phys Rev B* 1984; **30**: 870–875.
25. Ferrari AC, Robertson J. Resonant Raman spectroscopy of disordered, amorphous, and diamondlike carbon. *Phys Rev B* 2001; **64**: 075414.
26. Huang Q, Yu D, and Xu B, *et al.* Nanotwinned diamond with unprecedented hardness and stability. *Nature* 2014; **510**: 250–253.
27. Brookes CA, Brookes EJ. Diamond in perspective: A review of mechanical properties of natural diamond. *Diam Relat Mater* 1991; **1**: 13–17.
28. Donovan PE. Plastic flow and fracture of Pd₄₀Ni₄₀P₂₀ metallic glass under an indenter. *J Mater Sci* 1989; **24**: 523–535.
29. Oliver WC, Pharr GM. An improved technique for determining hardness and elastic modulus using load and displacement sensing indentation experiments. *J Mater Res* 1992; **7**: 1564–1583.
30. Lewandowski JJ, Greer AL. Temperature rise at shear bands in metallic glasses. *Nat Mater* 2006; **5**: 15–18.
31. Wheeler JM, Raghavan R, and Wehrs J, *et al.* Approaching the limits of strength: Measuring the uniaxial compressive strength of diamond at small scales. *Nano Lett* 2016; **16**: 812–816.
32. Lee C, Wei X, Kysar JW, Hone J. Measurement of the elastic properties and intrinsic strength of monolayer graphene. *Science* 2008; **321**: 385–388.
33. Roundy D, Cohen ML. Ideal strength of diamond, Si, and Ge. *Phys Rev B* 2001; **64**: 212103.
34. Mao WL, Mao H, and Eng PJ, *et al.* Bonding change in compressed superhard graphite. *Science* 2003; **302**: 425–427.
35. Yamanaka S, Kini NS, and Kubo A, *et al.* Topochemical 3D polymerization of C₆₀ under high pressure at elevated temperatures. *J Am Chem Soc* 2008; **130**: 4303–4309.
36. Avery P, Wang X, and Oses C, *et al.* Predicting superhard materials via a machine learning informed evolutionary structure search. *Npj Comput Mater* 2019; **5**: 89.

37. Zhao Z, Xu B, and Wang L-M, *et al.* Three dimensional carbon-nanotube polymers. *ACS Nano* 2011; **5**: 7226–7234.
38. Hu M, Zhao Z, and Tian F, *et al.* Compressed carbon nanotubes: A family of new multifunctional carbon allotropes. *Sci Rep* 2013; **3**: 1331.
39. Pappas DL, Saenger KL, and Bruley J, *et al.* Pulsed laser deposition of diamond-like carbon films. *J Appl Phys* 1992; **71**: 5675-5684.
40. Fallon PJ, Veerasamy VS, and Davis CA, *et al.* Properties of filtered-ion-beam-deposited diamondlike carbon as a function of ion energy. *Phys Rev B* 1993; **48**: 4777–4782.
41. Brazhkin VV, Lyapin AG, and Voloshin RN, *et al.* Mechanism of the formation of a diamond nanocomposite during transformations of C₆₀ fullerite at high pressure. *J Exp Theor Phys Lett* 1999; **69**: 869–875.
42. Kim DY, Stefanoski S, Kurakevych OO, Strobel TA. Synthesis of an open-framework allotrope of silicon. *Nat Mater* 2014; **14**: 169–173.
43. Soum-Glaude A, Thomas L, Tomasella E. Amorphous silicon carbide coatings grown by low frequency PACVD: Structural and mechanical description. *Surf Coat Technol* 2006; **200**: 6425–6429.
44. Han Z, Li G, Tian J, Gu M. Microstructure and mechanical properties of boron carbide thin films. *Mater Lett* 2002; **57**: 899–903.
45. Seghi RR, Denry IL, Rosenstiel SF. Relative fracture toughness and hardness of new dental ceramics. *J Prosthet Dent* 1995; **74**: 145–150.
46. Gaskins JT, Hopkins PE, and Merrill DR, *et al.*, Review—investigation and review of the thermal, mechanical, electrical, optical, and structural properties of atomic layer deposited High-*k* dielectrics: beryllium oxide, aluminum oxide, hafnium oxide, and aluminum nitride. *ECS J Solid State Sci Technol* 2017; **6**: N189–N208.
47. Tiegel M, Hosseinabadi R, and Kuhn S, *et al.* Young's modulus, Vickers hardness and indentation fracture toughness of alumino silicate glasses. *Ceram Int* 2015; **41**: 7267–7275.

FUNDING

This work is supported by the National Key R&D Program of China (2018YFA0703400) and National Science Foundation of China (Nos. 51722209, 51672238, 91963203, 51525205, and 51672239). Z. Zhao also acknowledges the support of 100 Talents Plan of Hebei Province (E2016100013) and NSF for Distinguished Young Scholars of Hebei Province of China (E2018203349), and Key R&D Program of Hebei Province of China (17211110D). A.V. Soldatov and V. Benavides acknowledge European Union funding via Erasmus+/DOCMASE Doctoral school (grant number “2011-0020”). K. Luo acknowledges the China Postdoctoral Science Foundation (2017M620097).

AUTHOR CONTRIBUTIONS

Z.Z., A.V.S and Y.T. conceived the idea of this project; S.Z., B.L., Y.G. and Z.Z. prepared the samples; Z.L. and M.D. prepared the micron-pillars and carried out the compressive strength measurements. S.Z., Z.Z., K.L. and Y.Z. measured the XRD and Raman spectra; S.Z., K.L., Y.G., B.L., G.G. and J.H. performed hardness measurements; S.Z. and Y.G. scanned the indentations through the atomic force microscope (AFM) and scanning electron microscope (SEM); K.S, L.S. and G.Y. measured the absorption spectra; B.Z. and B.L. prepared the TEM samples using the focused ion beam (FIB) technology; W.H., A.N., Z.L. and B.L. conducted TEM and EELS characterization; Z.Z., S.Z., J.H., D.Y., B.X., Y.T., A.V.S., V.B., O.P.C., K.L., W.H., G.G., Y.L., X.Z. and B.W. analyzed the data; Z.Z., S.Z. and A.V.S. drafted the manuscript with contributions from all authors. S.Z., Z.L., K.L., J.H. and Y.G. contributed equally to this work.

COMPETING INTERESTS

The authors declare no competing financial interests.

SUPPLEMENTARY DATA

Supplementary data are available at *NSR* online.

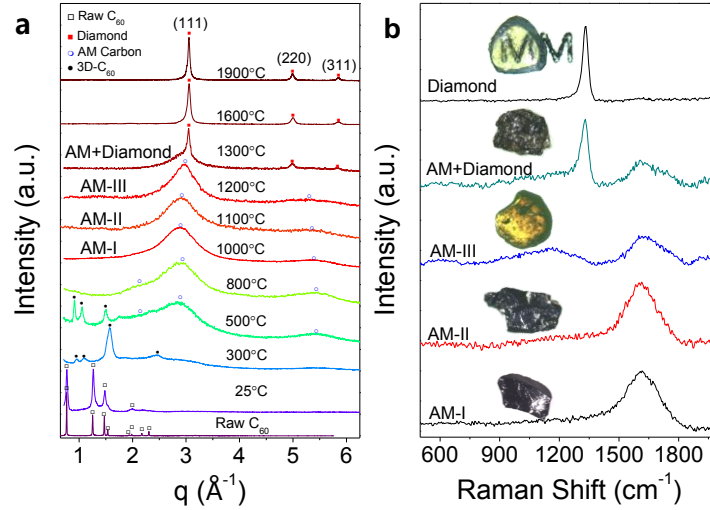


Figure 1. XRD patterns and Raman spectra of carbon phases collected at ambient condition. **a**, XRD patterns indicating phase transition path along $C_{60} \rightarrow 3D-C_{60} \rightarrow$ Amorphous carbon \rightarrow Diamond. The amorphous carbons depicted as AM-I, AM-II and AM-III, have one main diffraction peak at structure factor (q) of $\sim 3.0 \text{ \AA}^{-1}$ as well as another weak peak around 5.3 \AA^{-1} , which are clearly different from previously discovered low-density amorphous carbons from compressing C_{60} at relatively low pressures[16, 41]. **b**, UV Raman spectra of AM phases and AM-III-Diamond composite compared to Raman spectrum of Diamond. The insets are the optical photographs of recovered samples, displaying that AM-III is yellow-transparent and distinct from the black AM-I and AM-II.

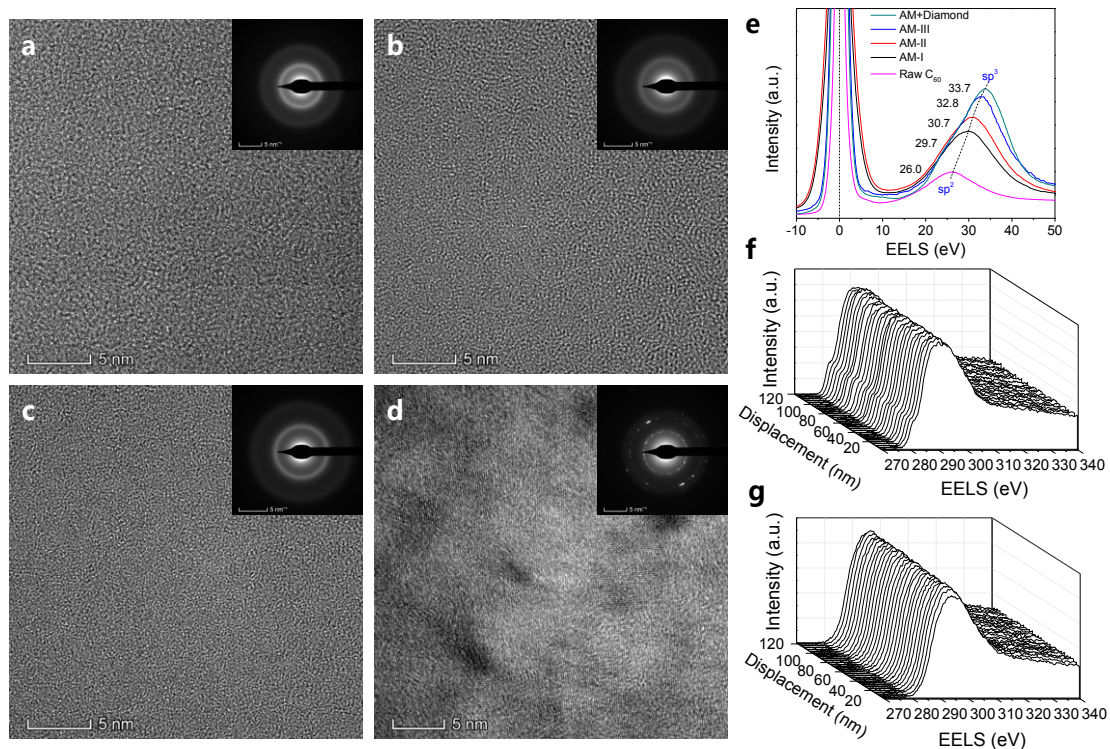


Figure 2. Microstructure and bonding of amorphous carbons. **a**, **b** and **c**, are HRTEM images of AM-I, AM-II and AM-III, respectively, showing their disorder characteristics. The amorphous fragment sizes in these AM carbons decrease gradually to several angstroms in AM-III. The insets: the corresponding SAED patterns, exhibit two diffuse rings near 2.1 Å and 1.2 Å. **d**, HRTEM image of AM/diamond composite. The results of HRTEM and SAED pattern indicate the formation of nanocrystalline diamond. **e**, Low loss EELS data. The position of plasmon peak is shifted from 26.0 eV to 33.7 eV, indicating the increase of sp^3 content in the samples. **f** and **g**, are the EELS line scans conducted in STEM mode along ~120 nm long lines with 1 nm step and energy resolution of 0.6 eV in a randomly selected regions of the AM-I and AM-III samples, respectively, showing the bonding homogeneity in their microstructures.

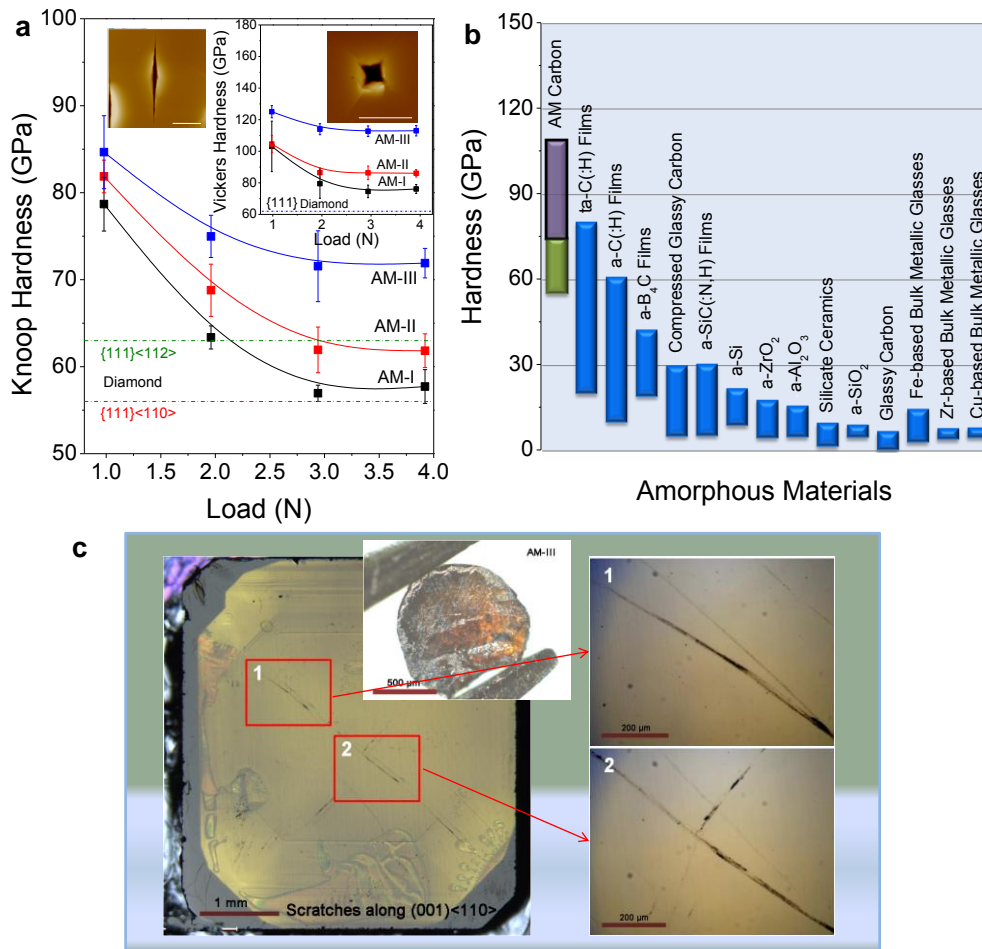


Figure 3. Hardness of amorphous carbons, compared with other known materials, and scratches on diamond (001) face indented by AM-III. **a**, Knoop hardness (H_K) as a function of applied loads. Left inset: AFM image of Knoop indentation of AM-III phase after unloading from 3.92 N. Right inset: Vickers hardness (H_V) of AM phases as a function of applied load and AFM image of Vickers indentation of AM-III sample after unloading from 2.94 N. The scale bars in indentation images are 10 μm . Error bars of hardness indicate s.d. ($n=5$). The dashed lines indicate H_V and H_K of (111) plane of natural diamond crystal. **b**, Hardness of different amorphous materials[2, 3, 7, 10, 29, 43–47]. Green and violet columns indicate H_K and H_V of AM carbons, respectively. Considering the hardness of film materials are characterized by nanoindentation hardness (H_N), the H_N of AM carbons was also measured, and AM-III has high H_N of 103 GPa, exceeding that (80.2 GPa) of ta-C films[7]. **c**, Scratches left on the (001) face of diamond by using AM-III sample displayed in the inset as an indenter (left image), indicating the ultrahard nature of the material. The zoomed-in right images are corresponding to the areas marked by red rectangles in the left image, displaying the scratches in more detail.

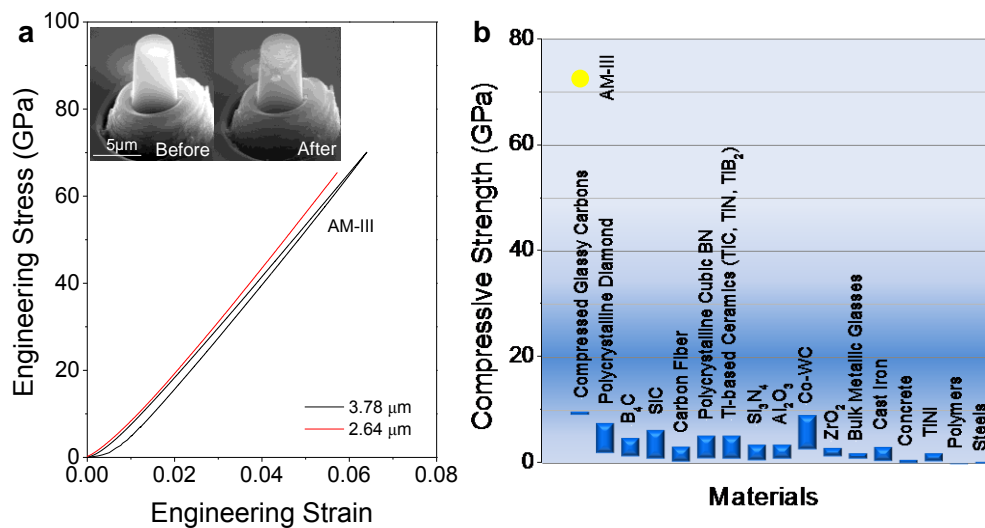


Figure 4. Strength of amorphous carbons, compared with other known materials. **a**, Engineering stress-strain curves recorded during uniaxial compressing micron-sized AM-III pillars. The insets are the SEM images of the pillar with diameter of 3.78 μm before and after compression. There was almost no size change, but some wrinkles produced on upper part of the pillar are like the shear bands formed in metallic glasses[30]. **b**, Comparison of compressive strength for various materials[10]. The results demonstrate that AM carbons are the hardest and strongest amorphous materials known to date.

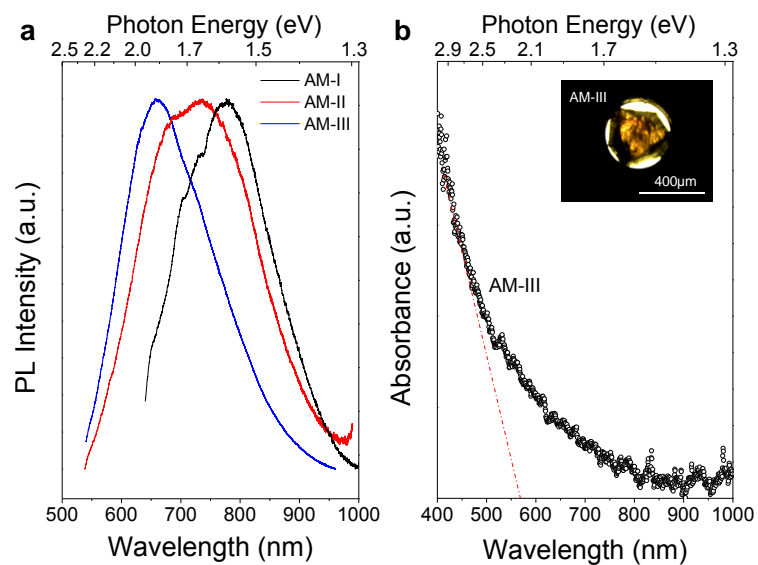


Figure 5. Optical properties and bandgaps of amorphous carbons. **a**, PL spectra measured at ambient condition. The AM-I spectrum is excited by 633 nm laser, the AM-II and AM-III spectra are excited by 532 nm laser. The bandgaps of AMs estimated from PL spectra are between 1.5 and 2.2 eV, illustrating their semiconducting nature. **b**, Absorption spectrum of AM-III. The absorption edge of AM-III is at ~570 nm, corresponding to optical bandgap value of 2.15 eV. The inset shows an optical microscope view of a piece of transparent AM-III material placed inside the hole of a gasket which is mounted inside the diamond-anvil cell (DAC).

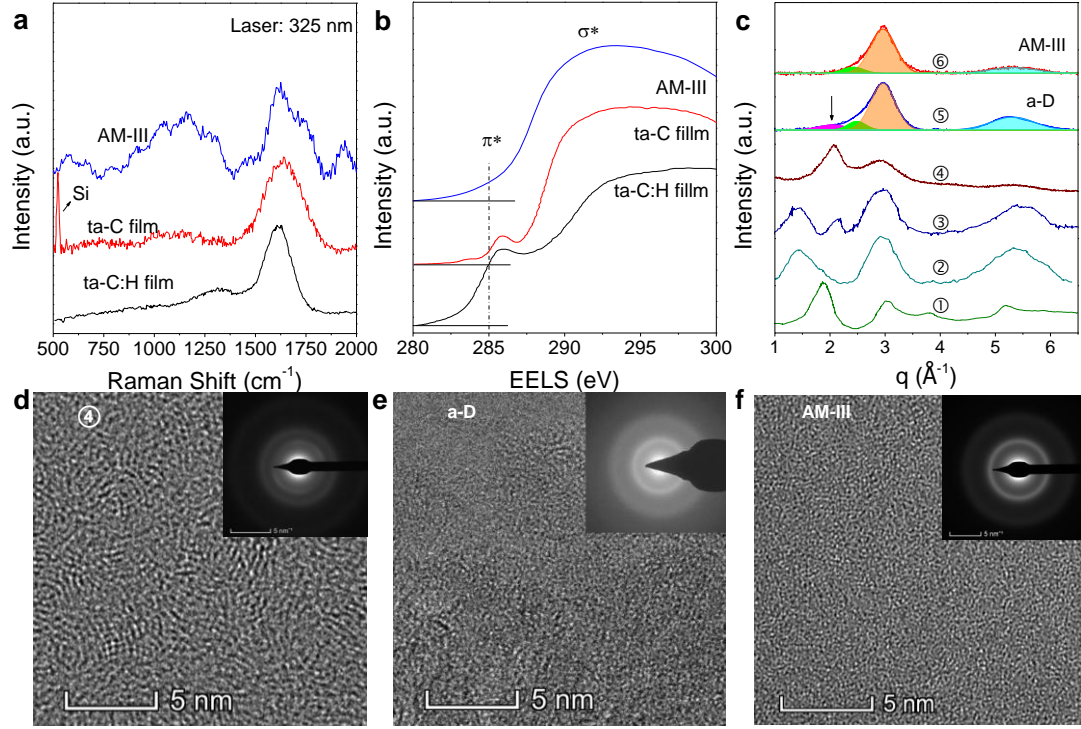


Figure 6. Comparison of AM-III currently discovered with other AM carbon materials including ta-C(:H) films[7, 25, 39, 40], AM carbons from compressing C_{60} [16, 41] and a-D from compressing glassy carbon[11]. **a**, Raman spectra. The AM-III shows an obvious T band around $900\sim 1300\text{ cm}^{-1}$ compared to ta-C(:H) films[7, 25]. **b**, EELS showing intensity difference of the peak around 285 eV, representing the different sp^3 contents of AM-III and ta-C(:H) films[39, 40]. **c**, XRD of various AM carbons recovered from compressing C_{60} at p, T conditions: ① 8 GPa, 1200 °C[16, 41]; ② 12.5 GPa, 500 °C[16, 41]; ③ 13.5 GPa, 1000 °C[16, 41]; ④ 15 GPa, 800 °C (our data); ⑥ 25 GPa, 1200 °C (AM-III, our data). Furthermore, the background-free XRD of a-D recovered from compressing GC at 50 GPa, 1527 °C[11] is also shown as ⑤ for comparison, showing a residual graphite-like diffraction peak near $q\sim 2.0\text{ \AA}^{-1}$. **d**, **e**, and **f**, are HRTEM images of AM carbon from compressing C_{60} at p, T condition ④, a-D[11] and AM-III, respectively, showing their obvious microstructural differences.

Supplementary Information

Discovery of carbon-based strongest and hardest amorphous material

**Shuangshuang Zhang^{1†}, Zihé Li^{1†}, Kun Luo^{1,2†}, Julong He^{1†}, Yufei Gao^{1,2†},
Alexander V. Soldatov^{3,4,5}, Vicente Benavides³, Kaiyuan Shi⁶, Anmin Nie¹, Bin
Zhang¹, Wentao Hu¹, Mengdong Ma¹, Yong Liu², Bin Wen¹, Guoying Gao¹,
Bing Liu¹, Yang Zhang^{1,2}, Dongli Yu¹, Xiang-Feng Zhou¹, Zhisheng Zhao^{1*}, Bo
Xu¹, Lei Su⁶, Guoqiang Yang⁶, Olga P. Chernogorova⁷, Yongjun Tian^{1*}**

¹Center for High Pressure Science (CHiPS), State Key Laboratory of Metastable Materials Science and Technology, Yanshan University, Qinhuangdao, Hebei 066004, China

²Hebei Key Laboratory of Microstructural Material Physics, School of Science, Yanshan University, Qinhuangdao 066004, China

³Department of Engineering Sciences and Mathematics, Luleå University of Technology, SE-97187 Luleå, Sweden

⁴Department of Physics, Harvard University, Cambridge, MA 02138, USA

⁵Center for High Pressure Science and Technology Advanced Research, Shanghai 201203, China

⁶Key Laboratory of Photochemistry, Institute of Chemistry, University of Chinese Academy of Sciences, Chinese Academy of Sciences, Beijing, 100190, China

⁷Baikov Institute of Metallurgy and Materials Science, Moscow 119334, Russia

* Corresponding authors: zzhao@ysu.edu.cn (Z.Z.) or fhcl@ysu.edu.cn (Y.T.). †These authors contributed equally to this work.

Table of Contents

- **Figure S1.** Structure factors $S(q)$ (a), and pair distribution functions $G(r)$ (b) of the AM phases quenched from synthesis pressure of 25 GPa and various temperatures.
- **Figure S2.** XRD patterns of carbon phases synthesized at 15 GPa and different temperatures from collapsed C_{60} fullerenes collected after subsequent samples quenching to ambient conditions.
- **Figure S3.** UV Raman spectra of the carbon phases quenched from synthesis pressure of 25 GPa and various temperatures.
- **Figure S4.** EEL spectra (EELS) of pristine C_{60} , amorphous carbons, and amorphous carbon/diamond composite.
- **Figure S5.** XRD and EELS comparisons of AM carbons currently discovered with a-D from compressing glassy carbon[9], nano-diamond[9] and CVD diamond[10].
- **Figure S6.** Images of Knoop, Vickers and Berkovich indentations.
- **Figure S7.** Nanoindentation hardness and Young's moduli of AM-I, AM-II and AM-III.
- **Figure S8.** Vickers (H_V) and Knoop (H_K) hardness of different crystal faces of single crystalline diamond.
- **Figure S9.** Vickers indentation morphologies of AM-III after unloading from different loads (a, b) and the corresponding indentation profiles along the diagonals scanned by AFM (c).
- **Figure S10.** *In-situ* compression/decompression testing of an AM-III micron-sized pillar.
- **Figure S11.** Thermogravimetric analysis (TGA) (top panel) and differential scanning calorimetry (DSC) heat flow data (bottom panel) collected from AM-III phase in air.

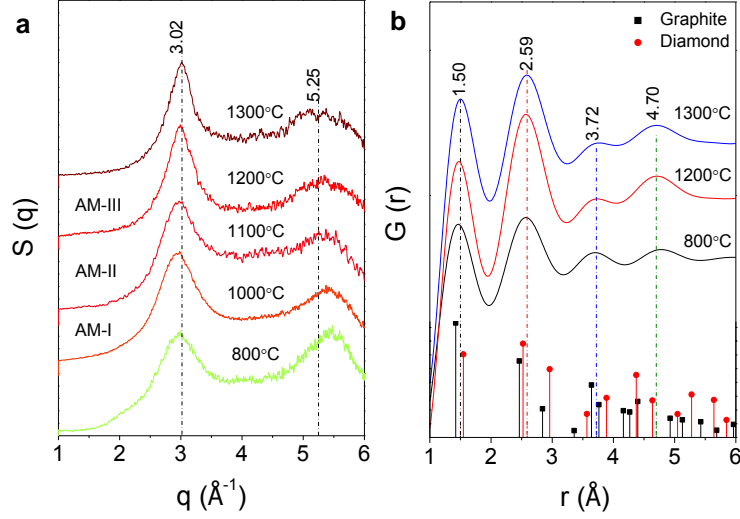


Figure S1. Structure factors $S(q)$ (a), and pair distribution functions $G(r)$ (b) of the AM phases quenched from synthesis pressure of 25 GPa and various temperatures. Two broad diffraction peaks are visible at positions of ~ 3.0 and 5.3 \AA^{-1} , respectively. With the synthesis temperature increase, the first and second peak shift to higher- and lower q , gradually approaching the (111) and (220) reflections position of diamond at $q=3.05$ and 4.98 \AA^{-1} , respectively. The dashed lines give an indication of the peak shifts. The positions of first nearest neighbor peaks in $G(r)$ shift to higher r with the synthesis temperature increase, which corresponds to an average bond lengths increase from 1.472 \AA to 1.50 \AA for the AM carbons. The bond lengths of the AM carbons lie between the bond length of sp^2 (1.422 \AA) and sp^3 (1.545 \AA) carbons in graphene and diamond, respectively, thus, demonstrating presence of both hybridizations in the AM carbon phases under investigation. Note: the sample recovered from $1300 \text{ }^\circ\text{C}$ is composed of the AM carbon and diamond, but only the AM carbon component derives the $S(q)$ and $G(r)$ presented in panel b. The $G(r)$ of graphite and diamond are also shown for comparison.

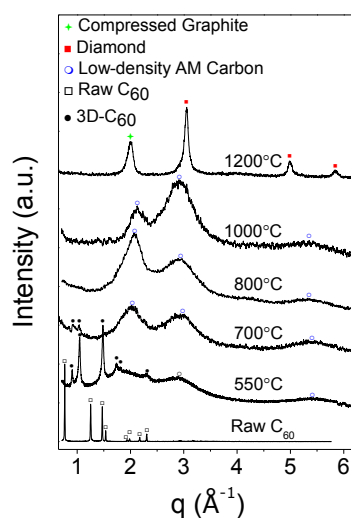


Figure S2. XRD patterns of carbon phases synthesized at 15 GPa and different temperatures from collapsed C₆₀ fullerenes collected after subsequent samples quenching to ambient conditions. With the increased synthesis temperatures, the resulting phase transition path is C₆₀ → 3D-C₆₀ → Amorphous carbons → Diamond/compressed graphite composite. At this synthesis condition, the amorphous carbons recovered from 700-1000 °C has two main diffraction peaks at around 2.0 Å⁻¹ and 2.9 Å⁻¹, as well as one minor peak at about 5.3 Å⁻¹. In contrast, the amorphous carbons recovered from 25 GPa and 1000-1200 °C have only two diffraction peaks, at around 3.0 Å⁻¹ and 5.3 Å⁻¹. The diffraction peak centered around 2.0 Å⁻¹ corresponds to the large graphite interlayer-like distance of ~3.1 Å, that implies the amorphous carbons quenched from 15 GPa have densities lower than their counterparts quenched from 25 GPa.

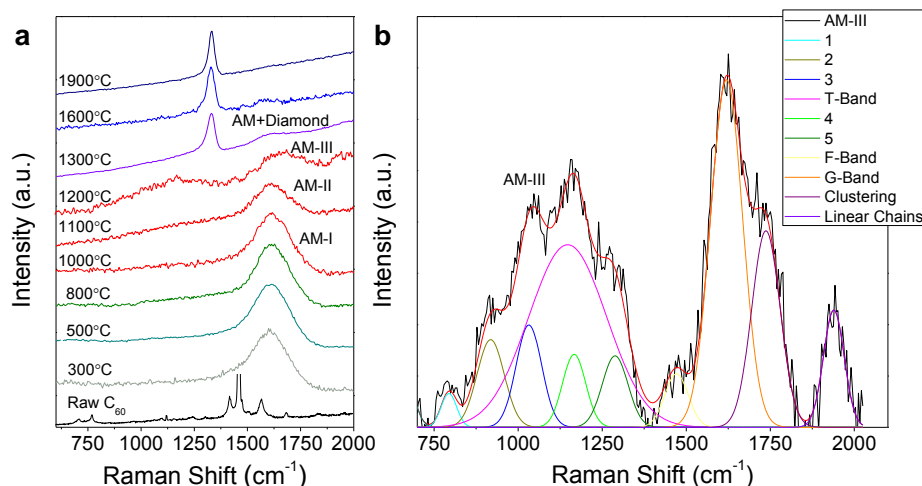


Figure S3. UV Raman spectra of the carbon phases quenched from synthesis pressure of 25 GPa and various temperatures. **a**, The fluorescence background was not removed. Above 1300 °C, the Raman peak of diamond appeared at 1330 cm⁻¹. Below that synthesis temperature, all the spectra exhibit characteristic of sp^2 carbons broad G band located at about 1600 cm⁻¹. An additional broad peak appears at around 900~1300 cm⁻¹ in AM-III, which is commonly known as T band indicating the high sp^3 carbons fraction in this material. **b**, Decomposition of the UV Raman spectrum of the AM-III and peaks assignment. Peaks 1 to 5: UV Raman spectroscopy of hydrocarbons[1] reveals similar vibrations that can be related to different configuration of fused aromatic rings. In case of AM-III phase it is likely that the aromatic rings are linked to each other (fused) via sp^3 carbons and randomly oriented in the material; F Band: this vibration is related to pentagonal rings (analogous to Ag(2) mode in C₆₀). F-band was observed in fullerene-like disordered carbon systems[2], like glassy carbon[3], fullerene-like amorphous carbon thin films[4, 5] and nano-clustered graphene[6]; G Band peak position reflects a mixture of linear chains and fused rings fragments[2]; “C-clustering” peak at 1740 cm⁻¹ corresponds to tiny graphene clusters residues in highly disordered sp^3/sp^2 carbon systems, for example, carbon nanodots[7]; peak at 1940 cm⁻¹ is tentatively assigned to short linear carbon chains[2, 8].

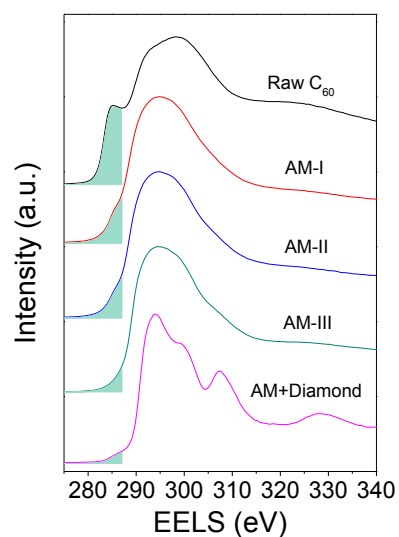


Figure S4. EEL spectra (EELS) of pristine C₆₀, amorphous carbons, and amorphous carbon/diamond composite. Contribution of the sp^2 carbons in the spectra represented by the 1s- π^* transition (green-shaded areas) gradually decreases with increase of the synthesis temperature (top to bottom).

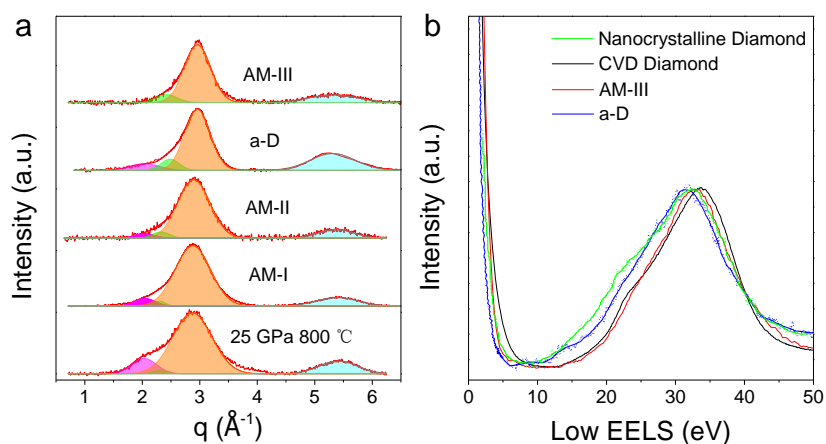


Figure S5. XRD and EELS comparisons of AM carbons currently discovered with a-D from compressing glassy carbon[9], nano-diamond[9] and CVD diamond[10]. **a**, XRD fitting peak results of AM carbons and a-D. The magenta peak at $q \approx 2.0 \text{ \AA}^{-1}$ is from the interlayer diffraction signal of residual graphite-like nanoclusters in amorphous carbons including AM-I, AM-II, AM phase from compressing C60 at 25 GPa, 800 °C as well as a-D[9]. However, this peak disappears in AM-III, demonstrating a completely different and new short-range ordered structure. Please also see the obvious difference of Raman spectra between AM-III and AM-I/AM-II (Figs. 1 and S3). **b**, Low EELS showing that the plasmon peak position in AM-III is higher than that in a-D[9] and close to that of CVD diamond[10]. More differences between AM-III and other amorphous carbons are shown in Fig. 6 and discussed in detail in the text.

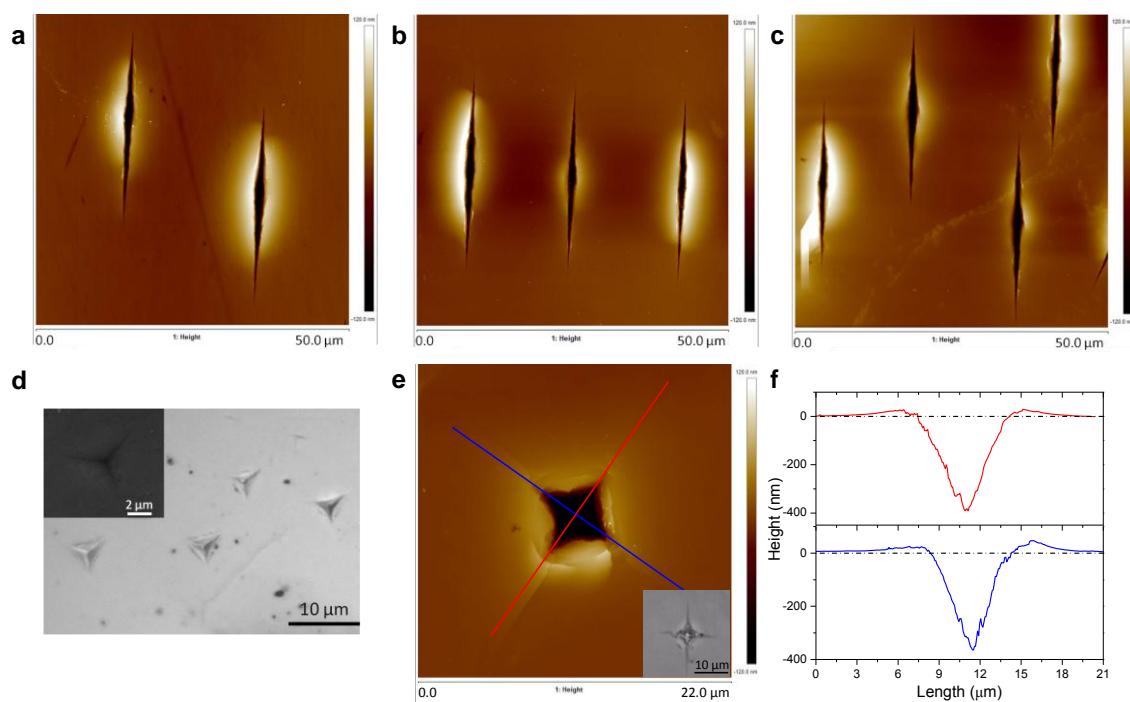


Figure S6. Images of Knoop, Vickers and Berkovich indentations. **a**, **b** and **c**, AFM images of Knoop indentations on surfaces of AM-I, AM-II and AM-III phases, respectively. In all cases, the applied load was 3.92 N. **d**, Optical and SEM images of AM-III phase surface after indentation at a load of 0.98 N with Berkovich-type pyramid probe. **e**, AFM image of a residual indentation by the Vickers probe on AM-III surface at a load of 2.94 N. The inset shows corresponding optical photograph of the indentation. **f**, AFM scan of the indentation profile in **e** along the diagonals.

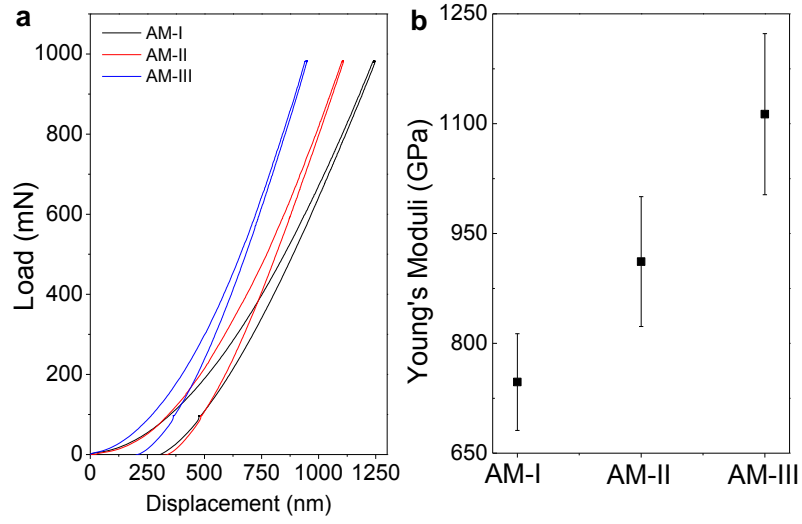


Figure S7. Nanoindentation hardness and Young's moduli of AM-I, AM-II and AM-III. a, Loading/unloading displacement curves during indentation measurement. The derived hardness (H_N) at a peak load of 0.98 N are 76 ± 3.4 , 90 ± 7.9 , and 103 ± 2.3 GPa, respectively, which are comparable to the hardness values determined by Vickers method. **b,** Young's moduli (E) of the amorphous carbons. By assuming Poisson's ratio of 0.2, the estimated E of AM-I, AM-II and AM-III are 747 ± 66 , 912 ± 89 , 1113 ± 110 GPa, respectively.

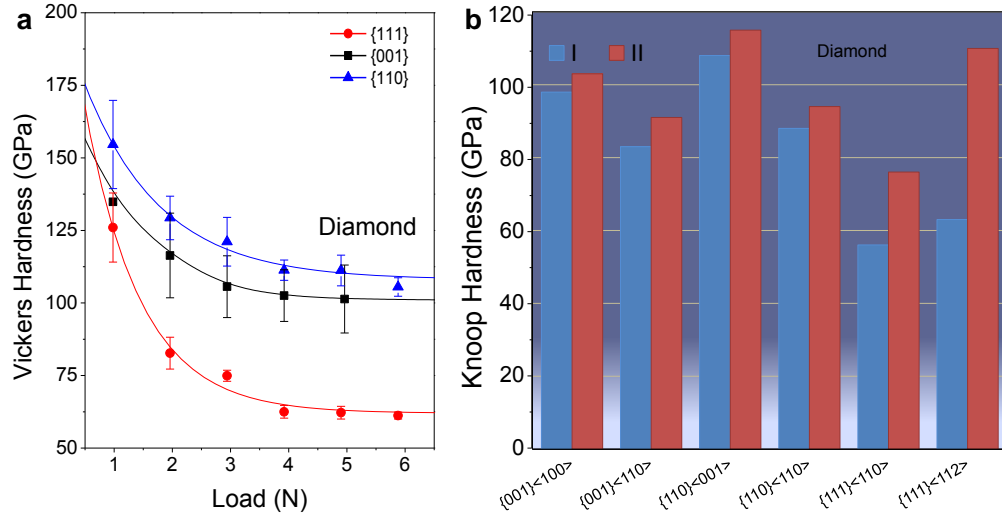


Figure S8. Vickers (H_V) and Knoop (H_K) hardness of different crystal faces of single crystalline diamond. a, H_V as a function of applied load. The asymptotic H_V values of $\{111\}$ and $\{110\}$ faces of natural diamond are 62 and 111 GPa, respectively[11]. In this work we determined the asymptotic H_V of $\{001\}$ face of synthetic diamond at 103 GPa. b, H_K of natural diamond along different crystallographic directions. The data in the figure are from the literature[12] (I: Type Ia natural diamond, and II: Type IIa natural diamond).

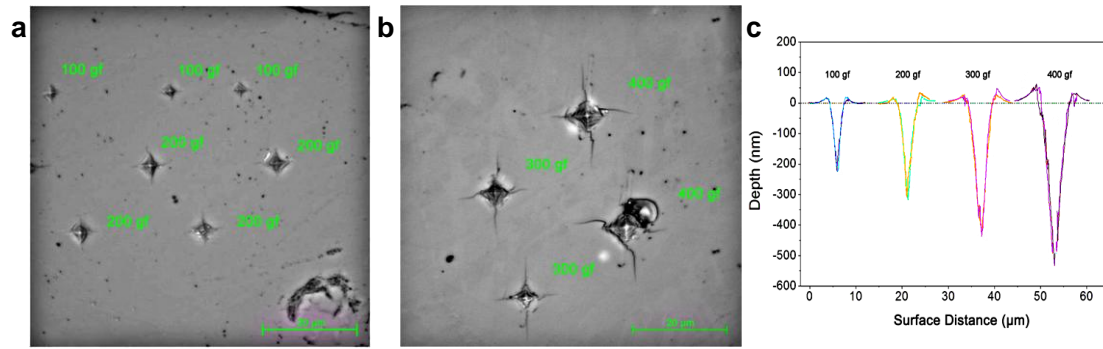


Figure S9. Vickers indentation morphologies of AM-III after unloading from different loads (a, b) and the corresponding indentation profiles along the diagonals scanned by AFM (c).

At small loads, there is no obvious indentation cracks, indicating the dominant plastic deformation. At the large loads, the radial and lateral cracks as well as peeling zones can be found around the indentations, demonstrating the plastic-to-brittle transition[13]. For all the loads, the displaced material flows up around the indenter to form a raised pile-up, indicating the occurrence of plastic flow in these cases.

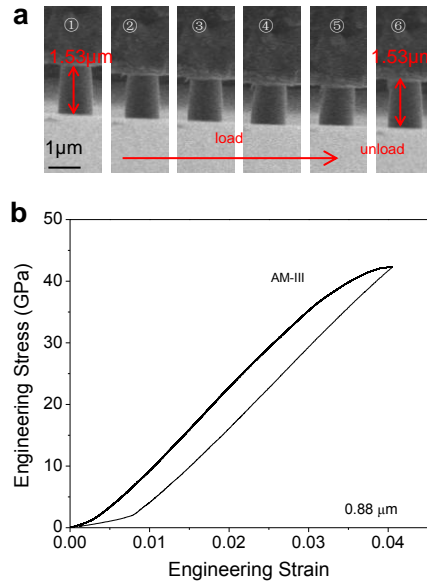


Figure S10. *In-situ* compression/decompression testing of an AM-III micron-sized pillar. a, *In-situ* SEM images exhibit the pillar height change during compression (①-⑤) and after decompression ⑥. The micron-sized pillar with a top diameter of 0.88 μm was shortened during compression, and the deformation was completely recovered after unloading. b, Engineering stress-strain curve. Notably, the compression curve shows nonlinearity at the maximum load, likely due to tilting and bending of the pillar.

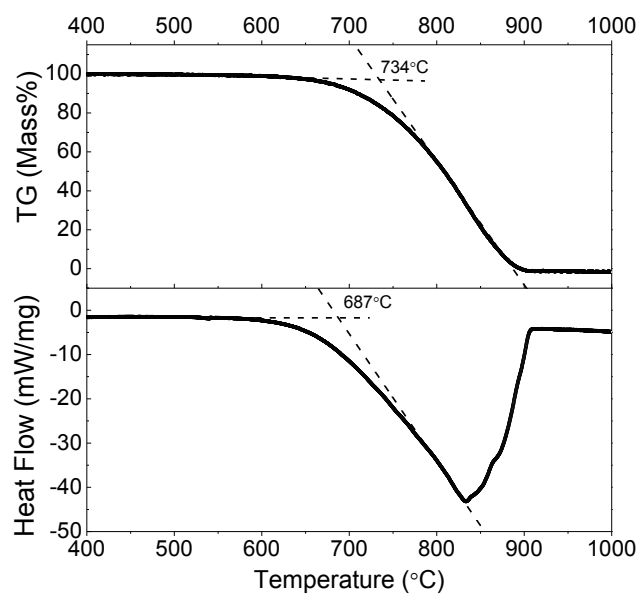


Figure S11. Thermogravimetric analysis (TGA) (top panel) and differential scanning calorimetry (DSC) heat flow data (bottom panel) collected from AM-III phase in air. The oxidation onset temperatures were determined at 734 °C and 687 °C, from TGA and DSC data, respectively. The thermal stability of amorphous carbon is comparable to that of crystalline diamond[9].

REFERENCES

1. Loppnow GR, Shoute L, and Schmidt KJ, *et al.* UV Raman spectroscopy of hydrocarbons. *Phil Trans R Soc Lond A* 2004; **362**: 2461–2476.
2. Ferrari AC, Robertson J. Resonant Raman spectroscopy of disordered, amorphous, and diamondlike carbon. *Phys Rev B* 2001; **64**: 075414.
3. Solopova NA, Dubrovinskaia N, Dubrovinsky L. Raman spectroscopy of glassy carbon up to 60 GPa. *Appl Phys Lett* 2013; **102**: 121909.
4. Wang Q, Wang C, and Wang Z, *et al.* Fullerene nanostructure-induced excellent mechanical properties in hydrogenated amorphous carbon. *Appl Phys Lett* 2007; **91**: 141902.
5. Dennison JR, Doyle TE. An embedded ring approach to the vibrational dynamics of low-dimensional amorphous solids with applications to graphitic carbon materials. *Carbon* 1997; **35**: 1465–1477.
6. Chernogorova O, Potapova I, and Drozdova E, *et al.* Structure and physical properties of nanoclustered graphene synthesized from C₆₀ fullerene under high pressure and high temperature. *Appl Phys Lett* 2014; **104**: 043110.
7. Bhattacharyya S, Ehrat F, and Urban P, *et al.* Effect of nitrogen atom positioning on the trade-off between emissive and photocatalytic properties of carbon dots. *Nat Commun* 2017; **8**: 1401.
8. Buntov EA, Zatsepin AF, Guseva MB, Ponomov YuS. 2D-ordered kinked carbyne chains: DFT modeling and Raman characterization. *Carbon* 2017; **117**: 271–278.
9. Zeng Z, Yang L, and Zeng Q, *et al.* Synthesis of quenchable amorphous diamond. *Nat Commun* 2017; **8**: 322.
10. Serin V, Beche E, and Abidate O, *et al.* Proceedings of the Fifth International Symposium on Diamond Materials. *Electrochem Soc Proc* 1998; **97–32**: 124126–141
11. Huang Q, Yu D, and Xu B, *et al.* Nanotwinned diamond with unprecedented hardness and stability. *Nature* 2014; **510**: 250–253.
12. Brookes CA, Brookes EJ. Diamond in perspective: A review of mechanical properties of natural diamond. *Diam Relat Mater* 1993; **1**: 13–17
13. Donovan PE. Plastic flow and fracture of Pd₄₀Ni₄₀P₂₀ metallic glass under an indenter. *J Mater Sci* 1989; **24**: 523–535.